Real-Time Guidance Provided by NOAA's Hurricane Research Division to Forecasters during Emily of 1993

Robert W. Burpee,* Sim D. Aberson,* Peter G. Black,* Mark DeMaria,*
James L. Franklin,* Joseph S. Griffin,* Samuel H. Houston,*
John Kaplan,* Stephen J. Lord,+ Frank D. Marks Jr.,*
Mark D. Powell,* and Hugh E. Willoughby*

Abstract

The Hurricane Research Division (HRD) is NOAA's primary component for research on tropical cyclones. In accomplishing research goals, many staff members have developed analysis procedures and forecast models that not only help improve the understanding of hurricane structure, motion, and intensity change, but also provide operational support for forecasters at the National Hurricane Center (NHC). During the 1993 hurricane season, HRD demonstrated three important real-time capabilities for the first time. These achievements included the successful transmission of a series of color radar reflectivity images from the NOAA research aircraft to NHC, the operational availability of objective mesoscale streamline and isotach analyses of a hurricane surface wind field, and the transition of the experimental dropwindsonde program on the periphery of hurricanes to a technology capable of supporting operational requirements. Examples of these and other real-time capabilities are presented for Hurricane Emily.

1. Introduction

An essential part of the mission of the National Oceanographic and Atmospheric Administration's (NOAA) Hurricane Research Division and its predecessor organizations (hereafter HRD) has been operational support for forecasters. Soon after the formation of the first federally funded hurricane research group in 1956, the division helped support the establishment of additional radiosonde stations in the Caribbean Basin, the mounting of cameras on coastal radars, and the installation of Weather Surveillance Radar–1957 (WSR-57) systems. HRD staff tested subjective techniques for improving synoptic analyses in the Tropics and examined the usefulness of vertically averaged winds for optimum forecasting of storm motion. Former directors of the organization Simpson (1980) and Gentry (1980) summarized important events during HRD's first 25 years.

Hurricane track forecasts began to improve soon after the research group, initially located in West Palm Beach, Florida, moved into the same building with forecasters at the National Hurricane Center (NHC) in Miami. During the eight years following collocation, Dunn et al. (1968) documented 10% and 12% reductions in the errors of the official 24-h hurricane forecasts in two oceanic areas adjacent to the Gulf and Atlantic coasts of the United States. They attributed the reduction in forecast track errors to close cooperation between researchers and forecasters and improved objective forecast techniques. Neumann's (1981) normalization of track errors from 1954–80 confirmed the forecast improvement. Although physical separation occurred in 1983, HRD has maintained space at NHC for development work.

HRD developed or supported development of hurricane track forecast models during the 1960s. The first models used statistical regression techniques (e.g., Miller et al. 1968) and were operational from 1964 to 1987. Project funds supported development of the first operational barotropic hurricane track forecast model (Sanders and Burpee 1968), which became operational in 1969. Later versions of the model provided guidance to forecasters through the late 1980s. The National Meteorological Center (NMC) has had the responsibility for new dynamical track models (e.g., Mathur 1991) since the early 1970s. As part of this responsibility, Lord (1991) added a synthetic vortex to improve the definition of the initial vortex in NMC's operational Global Spectral Model. Development of new operational hurricane modeling capability within NOAA is in progress at the Geophysical Fluid Dynamics Laboratory (GFDL) and HRD.

*Hurricane Research Division/AOML/NOAA, Miami, Florida.
+National Meteorological Center/NWS/NOAA, Camp Springs, Maryland.
Corresponding author address: Dr. Robert Burpee, Environmental Research Laboratories, Hurricane Research Division/NOAA, 4301 Rickenbacker Causeway, Miami, FL 33149-1097.
In final form 26 May 1994.

Kurihara et al. (1993) have been running a high-resolution three-dimensional hurricane model in a semioperational mode at GFDL and are modifying the model to run at NMC. HRD staff developed a multiply nested analysis and barotropic forecast system (DeMaria et al. 1992) that is competitive with the other operational track models (Aberson and DeMaria 1994) and are investigating the predictability of operational track model accuracy.

In the Atlantic basin, military aircraft began routine reconnaissance of tropical cyclones in 1944, and research aircraft started flying into hurricanes in the late 1950s. During the last 15 years, aircraft-to-satellite transmission capability has increased the potential of these planes to provide real-time observations to hurricane forecasters (Pifer et al. 1978). The basic data transmission includes occasional descriptive messages and flight-level wind and thermodynamic observations recorded at 1-min intervals on U.S. Air Force Reserve (AFRES) reconnaissance aircraft and 30-s intervals on NOAA research aircraft. Willoughby et al. (1989) describe analysis procedures that display the aircraft flight-level wind and pressure data in storm-relative coordinates for the forecasters. Using a workstation recently installed on the NOAA aircraft, Griffin et al. (1992) developed techniques for airborne analysis of dropwindsondes, radar reflectivity, and Doppler wind data for real-time transmission to NHC.

The National Weather Service (NWS) is implementing a modernized instrumentation network over the continental United States. NHC, however, issues many of its most important forecasts when hurricanes are over the ocean, beyond the range of the modernized network. To help improve operational forecasts and warnings, HRD has developed real-time analysis and modeling efforts that optimize use of sparse oceanic observations and special datasets from hurricane reconnaissance and research aircraft. This paper describes the current real-time analysis and forecasting capabilities and presents examples from Hurricane Emily of 1993. The real-time activities include analyzing flight-level and surface winds, compositing reflectivity patterns from aircraft radars, processing vertical soundings from dropwindsondes in the hurricane environment, forecasting storm motion with a barotropic forecast model, and predicting intensity change with a statistical regression model.

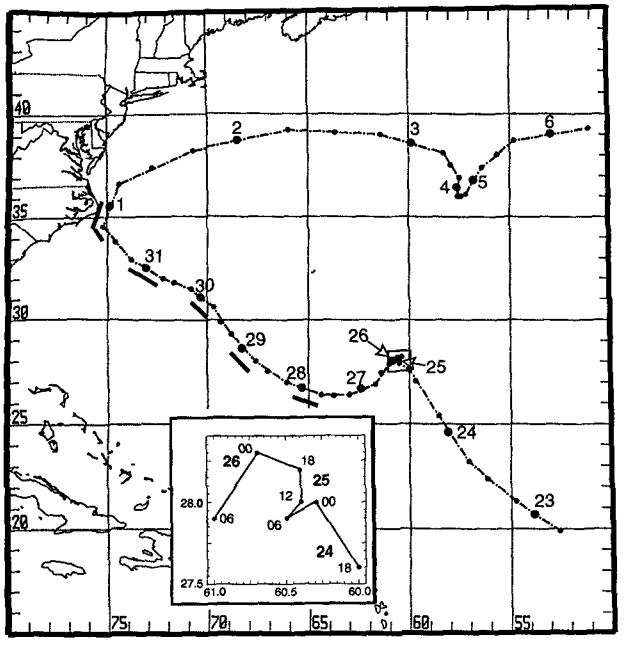

FIG. 1. NHC best-track positions for Hurricane Emily from 22 August to 6 September 1993. The large solid circles represent the 0000 UTC locations, and the small solid circles indicate the 0600, 1200, and 1800 UTC positions. The short lines paralleling the best track indicate the approximate times of the NOAA research flights. The enlarged area shows the cusp in the track on 25 and 26 August.

2. Hurricane Emily

The precursor of Emily was a cloud cluster associated with an easterly wave of African origin. Satellite images showed that the convective area in the wave's trough developed rotation and the characteristic cloud patterns of a tropical depression ~1300 km east-northeast of Puerto Rico on 22 August 1993. The depression moved northwestward for two days and then, on 25 and 26 August, its northward motion slowed and the track formed a cusp near 29°N, 60.5°W. As the system emerged from the cusp toward the west-southwest, NHC forecasters upgraded it to a tropical storm on the morning of 25 August and briefly to a minimal hurricane at midday on 26 August. After only 6 h, Emily weakened to a tropical storm but reached hurricane strength again on 27 August as it headed generally westward. Figure 1 shows Emily's "best track," the track of the storm center determined by poststorm analysis of all available observations, and the approximate times of the NOAA research flights.

Emily turned northwestward on 28 August in response to a midlatitude trough and, three days later, became a category 3 hurricane on the Saffir–Simpson scale (Simpson and Riehl 1981) with maximum surface wind speeds >50 m s^{-1}. At that time, Emily's eye was moving northward just to the east of the North Carolina coastline, with part of the western eyewall over the outer banks near Cape Hatteras. This was the closest that Emily came to land during its lifetime. After causing about $35 million in damage in coastal North Carolina and three deaths, the hurricane recurved and

remained over the ocean until it became extratropical on 6 September. Near the time of closest approach to land (CAL), reconnaissance aircraft measured Emily's lowest sea level pressure of 960 mb and strongest flight-level wind speed of 67 m s^{-1} at 500 m.

3. Analyses and forecasts

a. Vortex-scale evolution

Since the late 1980s, HRD has provided NHC with real-time analyses of the structure of the hurricane core based upon flight-level observations of wind and D value (Willoughby and Barry 1987; Willoughby et al. 1989). The analyses, plotted in storm-relative coordinates, enable forecasters to compare flight-level observations from different parts of a single flight with data from earlier flights. The D value (the departure of a selected isobaric height from the corresponding value in the standard atmosphere) is a proxy for pressure so that D-value variations at the center reflect changes in intensity and its sharpest radial gradient coincides with the strongest swirling wind. The motivation for this project has been the observationally based convective ring model, in which some tropical cyclones intensify by contraction of rings of convection that coincide with tangential wind maxima (Willoughby et al. 1982; Willoughby 1990). The analyses of flight-level data depict the structure of the vortex and, interpreted in terms of this model, provide input for statistical (Samsury and Rappaport 1991) and subjective forecasts of its evolution. Real-time analyses of the data from Emily illustrate these capabilities.

Figure 2 shows the history of Emily's MSLP (minimum sea level pressure) and eye radius. Emily experienced a long-term intensifying trend on 26 August as it emerged from the cusp in the track (Fig. 1), but the winds weakened below hurricane strength early on 27 August, while the pressure rose by a couple of millibars. As Emily curved back to the northwest, it regained hurricane strength. The 0000 UTC 28 August vortex message from the reconnaissance aircraft indicated that the MSLP had reached 981 mb, a fall of 36 mb during the previous 72 h. During the early stages of the formation of Emily's eyewall, a reconnaissance aircraft reported a tiny eye with a radius of only 2 km. About 10 h later, observers on a research aircraft and a second reconnaissance plane noted that the eye radius changed discontinuously from 14 to 5 km and then to 19 km in only 1.5 h. This unusual sequence of events may have resulted from differences in the organization of convection in Emily's developing eyewall or the replacement of the initial eyewall, labeled I in Fig. 2, by a slightly larger eyewall, labeled II. After the eye expansion, the MSLP remained within a millibar of 981 mb for 12 h and then fell only 6 mb in the subsequent 48 h. During the time the MSLP was steady, Hurricane Emily had a well-defined eye with a radius of ~20 km and maximum winds of 40 m s^{-1} at the 850-mb flight level (Fig. 3a).

Discontinuous expansion of the eye radius associated with an interruption of intensification, or even a weakening, is a commonly observed aspect of tropical cyclone development. It is termed "eyewall replacement" or "a concentric eyewall cycle." As the names imply, the expansion occurs when a second eyewall forms around the original one. Observational analyses (Willoughby et al. 1982) and analytical and numerical modeling studies (Shapiro and Willoughby 1982) suggest that the outer eyewall induces upper-level subsidence over the inner wall and interrupts the inflow of latent and sensible heat in the surface friction layer. Thus, as the outer eyewall strengthens, the inner eyewall weakens. Some intense hurricanes, such as Allen in 1980 or Diana in 1984, weaken abruptly when the inner eyewall disintegrates and the weaker outer eyewall becomes dominant. In weaker hurricanes with maximum winds <50 m s^{-1}, such as Emily before 31 August, the outer eyewall is usually as strong as the inner by the time of the replacement, so that the storm slows its intensification but seldom weakens appreciably (Willoughby et al. 1982; Willoughby 1990). Monitoring the development and propagation of convective rings requires careful attention to temporal and spatial continuity as well as comparison with radar reflectivity data. This procedure distinguishes persistent wind maxima that control the evolution of the vortex from asymmetric,

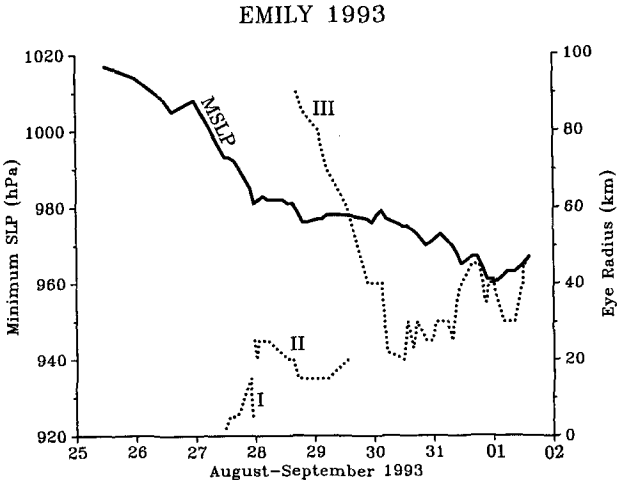

FIG. 2. The time history of Hurricane Emily's minimum sea level pressure (MSLP—solid line) and the radii of eyewalls I, II, and III (dotted line).

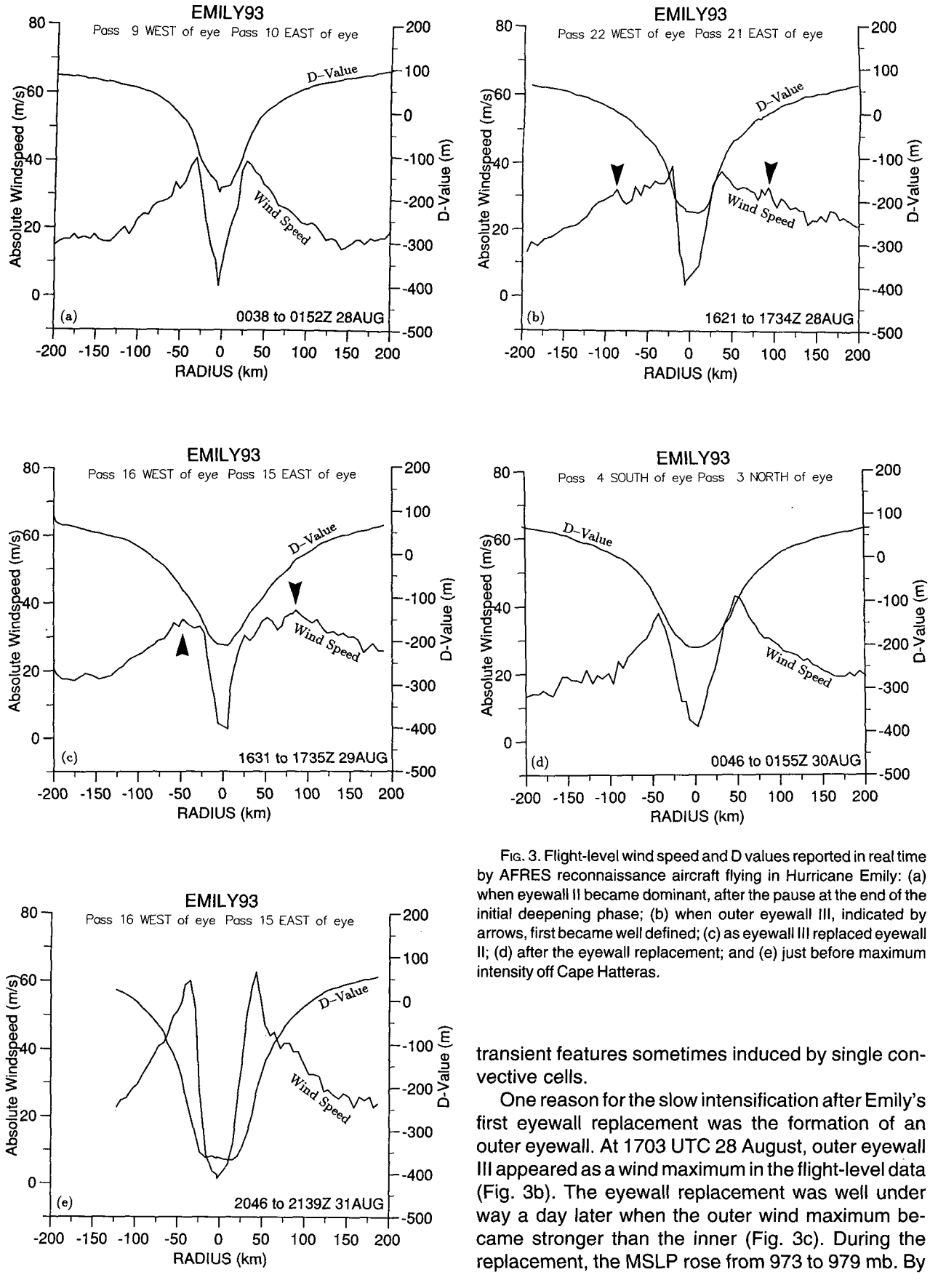

FIG. 3. Flight-level wind speed and D values reported in real time by AFRES reconnaissance aircraft flying in Hurricane Emily: (a) when eyewall II became dominant, after the pause at the end of the initial deepening phase; (b) when outer eyewall III, indicated by arrows, first became well defined; (c) as eyewall III replaced eyewall II; (d) after the eyewall replacement; and (e) just before maximum intensity off Cape Hatteras.

transient features sometimes induced by single convective cells.

One reason for the slow intensification after Emily's first eyewall replacement was the formation of an outer eyewall. At 1703 UTC 28 August, outer eyewall III appeared as a wind maximum in the flight-level data (Fig. 3b). The eyewall replacement was well under way a day later when the outer wind maximum became stronger than the inner (Fig. 3c). During the replacement, the MSLP rose from 973 to 979 mb. By

1200 UTC 30 August, the distributions of wind and D value had broadened, and only eyewall III remained with 40 m s^{-1} maximum wind at 50-km radius (Fig. 3d). Subsequently, the MSLP began to fall at a rate of a millibar every 3 h, reaching a minimum of 960 mb at 2349 UTC 31 August as Emily's track passed over the Gulf Stream close to Cape Hatteras. The maximum flight-level wind increased to >60 m s^{-1} at a 45-km radius (Fig. 3e). After Emily turned eastward, it maintained a large, slowly expanding eye with hurricane force winds for four days and eventually dissipated over the open Atlantic.

The replacement of Emily's eyewall II by eyewall III is a typical example of a concentric eyewall cycle in a weak hurricane (Willoughby et al. 1990). Samsury and Rappaport (1991) identified five distinct wind profile shapes in a study of hurricane observations recorded by research aircraft. The wind profiles in Figs. 3b–e are similar to their broad/dual, dual, and narrow categories, and the wind speed changes in the 36 h following the observation times are comparable to the average speed changes in their Table 1. Thus, the radial profiles of wind speed and D value provide forecasters with a valuable diagnostic tool that contains information on current storm structure and its future changes.

b. Radar reflectivity composites

Until Emily, forecasters did not have access to information describing the precipitation structure of hurricanes over the ocean unless a storm was within range of the coastal radar network. During 1991, Griffin et al. (1992) developed an airborne compositing technique for analyzing reflectivity data from the 5-cm radar mounted to the lower fuselage of the NOAA WP-3D research aircraft. The radar scans horizontally, has 4.1° vertical and 1.1° horizontal beamwidths, and records reflectivity only. Interpretation of reflectivity patterns from single rotations of the radar is difficult because of aircraft motion, intervening attenuation, and inadequate filling of the beam by precipitation particles. These problems are overcome by combining a sequence of radar scans in a composite map centered on the storm position (Marks 1985). Each 1-km^2 area of a composite contains the maximum reflectivity for the corresponding storm-relative area of all individual radar sweeps. Composites for 1–2 h provide an overall mesoscale perspective of the horizontal patterns of precipitation and a framework for interpretation of thermodynamic and kinematic observations.

Griffin et al. (1992) demonstrated their airborne radar compositing technique during eastern Pacific Hurricane Jimena of 1991; however, communication problems between computers prevented successful operational transmission of the data from the aircraft to NHC until the 1993 hurricane season. During Emily, radar reflectivities were composited on one of the WP-3D aircraft. The aircraft–satellite data link transmitted the composites to NHC, where the data were decoded and color prints prepared for the hurricane forecasters. They were able to examine the radar images less than 1 h after data transmission, while the aircraft was still airborne.

During the acquisition of the radar data, the aircraft was at altitudes of 5–6 km, which is just above the melting level. Reflectivities at these altitudes are usually much less than those below the melting level because of the predominance of ice particles, which are only 20% as reflective as raindrops (e.g., Marks 1985). Despite the lower reflectivities, the radar composites transmitted to NHC clearly identify the most important mesoscale precipitation features in Emily's core (Fig. 4).

The composites show the positions of the eyewall and major rainbands, the distance from the center of the radar eye to the ring of maximum reflectivities, and the increasing circular symmetry of the reflectivity in the core. The changes of these features with time are consistent with the concentric eyewall cycle described earlier in the radial profiles of the aircraft winds. On 28 August, a partial outer eyewall formed in the northern half of the storm at a radius of ~76 km from the center (Fig. 4b). The inner eyewall was well developed only on the northwest side of the storm. The limited extent of the inner eyewall was likely an indication that the outer eyewall was replacing it as in Hurricane Allen on 5 August 1980 (Willoughby et al. 1982). A radar composite is not available for 29 August because the mission that day was to obtain dropwindsonde observations on Emily's periphery at distances farther from the storm center than the radar's quantitative range. The radar images on 28 and 30 August (Figs. 4b and 4c) combined with the flight-level winds (Fig. 3) suggest that the inner eye in the composite on 28 August was replaced by the outer ring during this period.

The radar composites provided a tool for interpreting Emily's structure that was also consistent with satellite imagery (not shown). On 27 and 28 August, strong upper-tropospheric northerly winds advected cirrus from the rainbands in the storm's northern semicircle, toward the storm center, obscuring the eye evident in the radar composites. The sheared environment resulting from the northerly winds and low-level southeasterlies helped to maintain the asymmetric rainfall structure observed in other sheared hurricanes by Willoughby et al. (1984). After the upper-tropospheric winds weakened on 29 August, the storm began to strengthen, satellite imagery detected the eye, and the concentric eyewall cycle proceeded to a

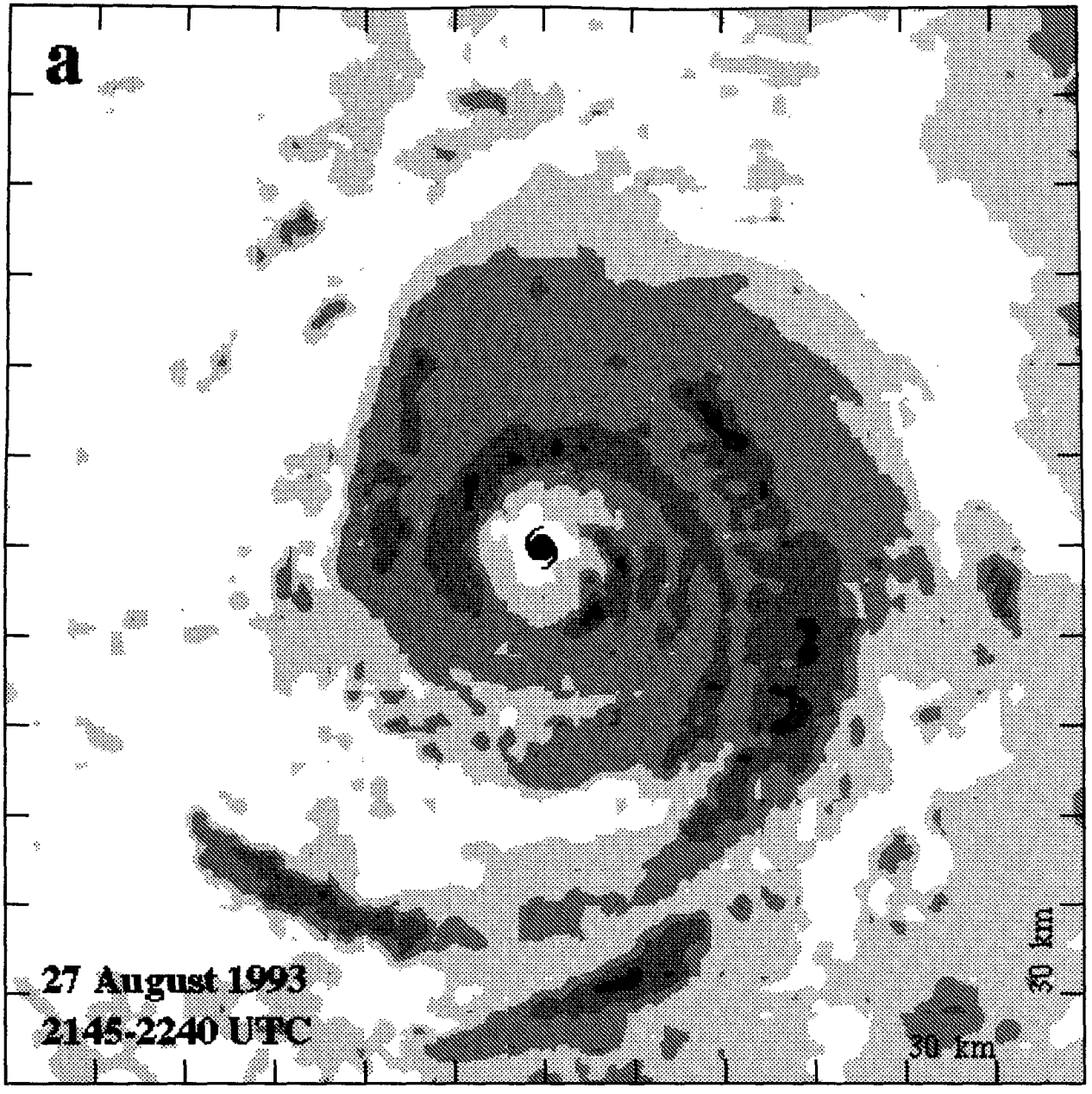

FIG. 4a. Radar composite calculated for 2145–2240 UTC 27 August. The contour levels indicate reflectivities below the minimum detectable signal (white) and greater than or equal to 15, 21, 28, 35, 41, and 48 dBZ. The domain is 360 km by 360 km and is positioned on the center of the eye at the time of the final radar sweep in the composite. North is at the top.

stage where the precipitation patterns in the core became more symmetric. The scenario of decreasing environmental shear accompanied by increasing intensity and symmetric structure is typical for mature hurricanes (Willoughby 1990; DeMaria and Kaplan 1994).

c. Real-time surface wind analyses

The length of coastline placed under hurricane watches and warnings largely depends upon typical errors in the track forecasts, but it is also affected by the horizontal extent of strong surface winds. Reduction in the uncertainty of the surface wind field can decrease economic losses associated with overwarning. Operational estimation of the surface wind field, however, has largely been a subjective process. The winds discussed in the marine and public advisories are the maximum sustained (1-min average) surface wind (V_{ms}) for oceanic exposure at a level of 10 m. Unfortunately, surface wind observations from

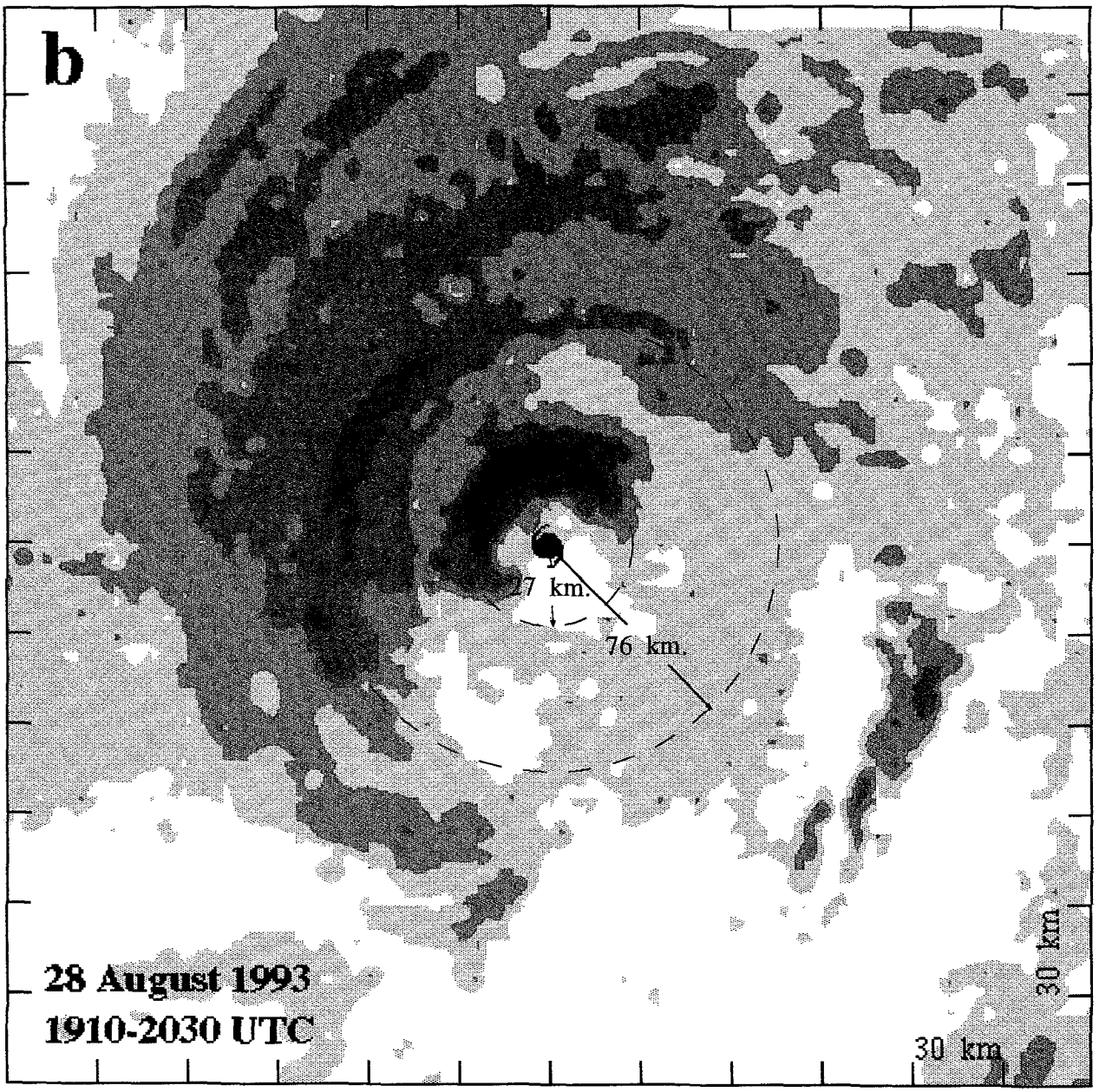

FIG. 4b. Same as Fig. 4a except for 1910–2030 UTC 28 August.

oceanic platforms are infrequent in hurricanes unless a storm happens to pass an instrumented National Data Buoy Center (NDBC) buoy, Coastal-Marine Automated Network (C-MAN) station, or ship of opportunity. Observations from reconnaissance and research aircraft help to fill in data gaps, but the aircraft and nearly all of the surface observations require adjustment for differences in anemometer height and averaging time.

For many years, hurricane forecasters have estimated surface winds from flight-level data using empirical relationships summarized by Powell et al. (1991). After the south Florida landfall of Hurricane Andrew, HRD began to develop a real-time data processing and analysis package for hurricane surface wind fields. The analysis package incorporates all available data and uses the spectral application of finite element representation (SAFER; for convenience, all model-related acronyms are also defined in Table 1) technique (Ooyama 1987; DeMaria et al. 1992). It not only depicts the wind field, but also provides information required for NHC's marine advisories, such as the radius of hurricane and gale force winds in each storm quadrant. A preliminary version of the analysis pack-

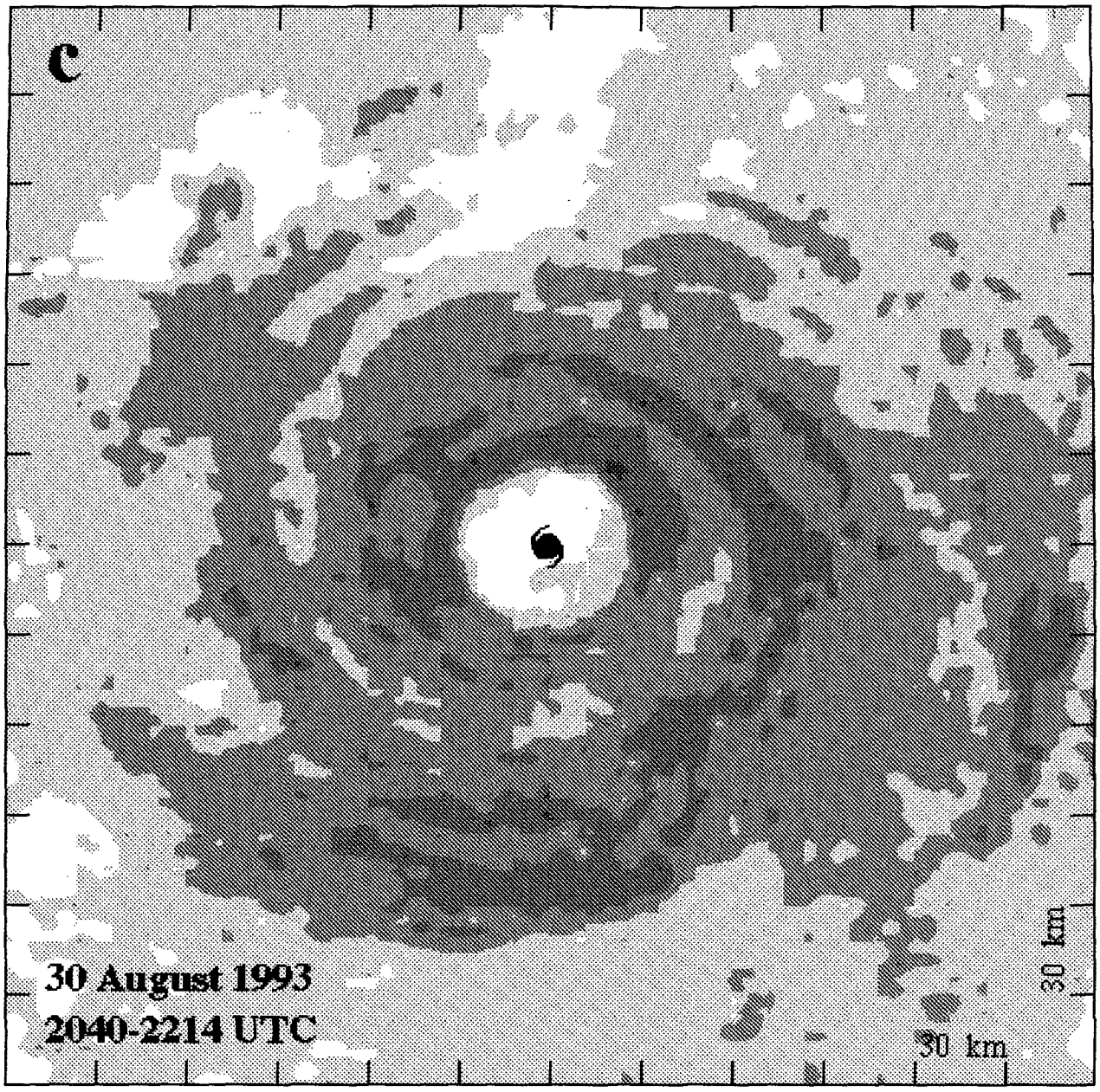

FIG. 4c. Same as Fig. 4a except for 2040–2214 UTC 30 August.

age was available as Emily approached the North Carolina coast. During the 12 h that Emily was near the coast, five analyses were completed and provided to the forecasters.

Observations were assimilated from a variety of coastal, offshore, and airborne platforms as indicated in Table 2. A research aircraft experiment was designed to evaluate new remote sensing instruments and methods for adjusting flight-level data to the surface. The AFRES reconnaissance and NOAA research aircraft were at 850 and 900 mb, respectively, levels that are typically near those of the maximum winds, and their flight tracks were offset by 45° in azimuth relative to the storm center.

Surface observations were adjusted to 10 m using a stability-dependent surface-layer model (Liu et al. 1979). The stability calculation is based upon the height of the wind measurement, the observed air temperature and mixing ratio, and the sea surface temperature. For observations with sampling periods >2 min, the V_{ms} was estimated using a gust factor relationship that depends upon the averaging time (Powell et al. 1991). Flight-level winds were adjusted to the 10-m level with Powell's (1980) diagnostic

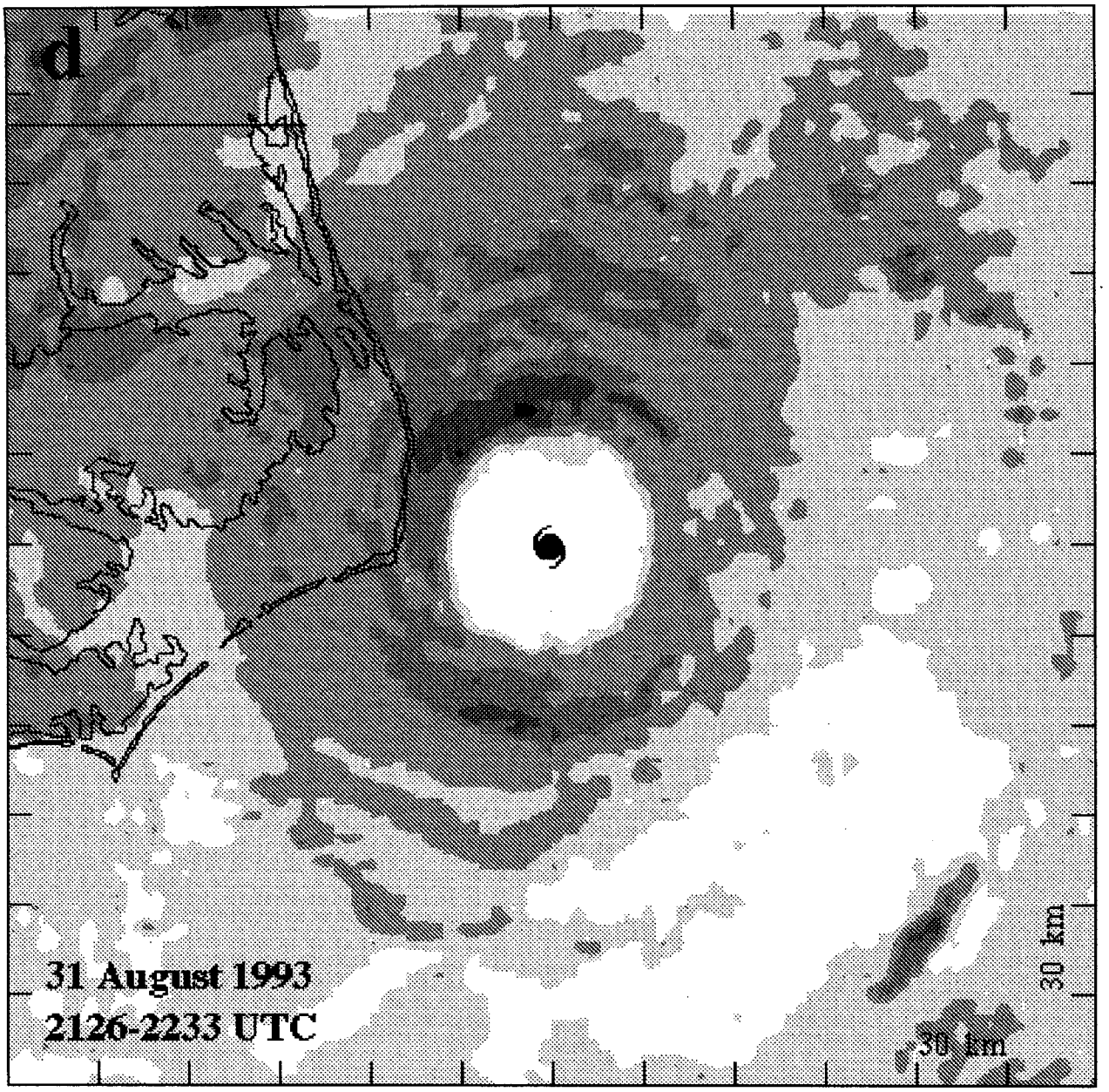

FIG. 4d. Same as Fig. 4a except for 2126–2233 UTC 31 August 1993.

marine planetary boundary layer model. The adjusted aircraft winds were assumed to represent 10-min averages and were increased about 10% by the gust factor relationship in determining the estimate of V_{ms}.

All data were then input to a graphical quality control application (Fig. 5) where they were examined relative to neighboring observations in storm- or earth-relative coordinates. Questionable data were flagged and included in the analysis only after subjective examination. Following quality control, the data were objectively analyzed on three nested meshes with the SAFER procedure. The three meshes are capable of resolving the extent of the gale force winds, the outer rainbands, and the maximum winds in the eyewall. The analyses presented here were usually 2 h old by the time they were produced. Further automation of data-gathering tasks, better access to real-time data sources, and faster communication lines and workstations will help cut these delays.

Most of the observations contributing to the analyses are aircraft data adjusted to the surface. Thus, the analyses are representative of oceanic exposure and are consistent with the maximum surface winds that would be expected at the coast. The dataset also

TABLE 1. Definitions of acronyms appearing in the text that are associated with hurricane track and intensity forecast models.

BAM	Beta and advection hurricane track forecast model
CAL	Closest approach to land
CLIPER	A climatology and persistence hurricane track forecast model
DVMX	Observed intensity change during previous 12 h; a term in SHIPS
NCHG	Intensity change model that assumes no change in intensity
NHC90	A statistical–dynamical hurricane track forecast model
NHC90-LATE	A version of NHC90
QLM	Quasi-Lagrangian hurricane track forecast model
PEFC	200-mb planetary eddy angular momentum flux convergence in SHIPS
REFC	200-mb relative eddy angular momentum flux convergence in SHIPS
SAFER	Spectral application of finite-element representation
SHIFOR	A climatology and persistence intensity change model
SHIPS	A statistical hurricane intensity prediction scheme
SHR	Vertical shear term in SHIPS
VICBAR	An analysis scheme and barotropic model using the SAFER method

TABLE 2. Coastal, oceanic, and airborne observing platforms used for the 2200 UTC 31 August 1993 analysis of Hurricane Emily. The table lists each station or platform name, platform type, height (z) of the wind observation, number (N) of observations available, and averaging time (T) for the wind. Platform types as follows: C-MAN—Coastal-Marine Automated Network; DoD—Department of Defense; FAA—Federal Aviation Administration; NWS—National Weather Service.

Station name	Platform type	z (m)	N	T (min)
NOAA42	Aircraft	1000	490	0.5
AF980	Aircraft	1500	157	1
CHLV2	C-MAN	43	18	(2/10)*
CLKN7	C-MAN	10	18	(2/10)*
DSLN7	C-MAN	47	12	(2/10)*
FPSN7	C-MAN	44	18	(2/10)*
41001	Buoy	5	18	(8.5/10)*
44014	Buoy	5	3	8.5
DGNB	Ship	19	1	1
WPGJ	Ship	19	1	1
Hatteras	NWS	10	4	1
Elizabeth City	FAA	10	4	1
Manteo	FAA	10	4	1
New Bern	FAA	10	4	1
Norfolk	FAA	10	4	1
Cherry Point	DoD	10	4	1
Norfolk-Navy	DoD	10	4	1

*The 2- or 8.5-min data available once per hour; continuous 10-min data available 6 times per hour.

includes several coastal stations with offshore or alongshore winds—for example, Cape Hatteras, Manteo, Elizabeth City, and Cape Lookout C-MAN—that account for slightly weaker winds on the western side of the analysis. Had Emily appeared likely to cross the coast, separate analyses would have been calculated with the aircraft observations adjusted to an open-terrain land exposure to depict the wind field experienced 2–5 km inland from the coastline. Inland and coastal observations with winds blowing from offshore also would have been adjusted to open-terrain exposure.

Two of the surface wind analyses are shown in Fig. 6 for the outer mesh. The first analysis (Fig. 6a) is for 1400 UTC 31 August and includes data plotted relative to the storm center for the previous 7 h. During that time interval, Emily moved north-northwestward as a weak category 2 hurricane on the Saffir–Simpson scale with maximum sustained surface winds of ~43 m s^{-1}. Analyses at 1730 and 1930 UTC (not shown) suggest that the winds were increasing.

By 2200 UTC, the surface isotachs (Fig. 6b) indicate that Emily was a dangerous category 3 hurricane with sustained eyewall winds >52 m s^{-1} offshore from Cape Hatteras. During the time window from 1800 to 2200 UTC when data were included in this analysis, Diamond Shoals Light C–MAN station (anemometer height of 47 m), located 36 km east of Hatteras, recorded a peak 10-min mean wind speed of 53 m s^{-1} and a 5-s mean gust of 66 m s^{-1}. Unfortunately these winds were not received in real time due to a transmission error. The surface-layer model would have adjusted the observed peak 10-min mean wind speed to a maximum 1-min sustained surface speed of 49 m s^{-1}, close to the value analyzed in Fig. 6b. The wind gust at Diamond Shoals was the third highest measured by an oceanic platform in an Atlantic hurricane and has been exceeded only by a 77 m s^{-1} gust at an oil rig (elevation 33 m) during Camille of 1969 and a 76 m s^{-1} gust at Fowey Rocks C-MAN (elevation 39 m) during Andrew of 1992. The analysis for 0200 UTC 1 September (not shown) indicated

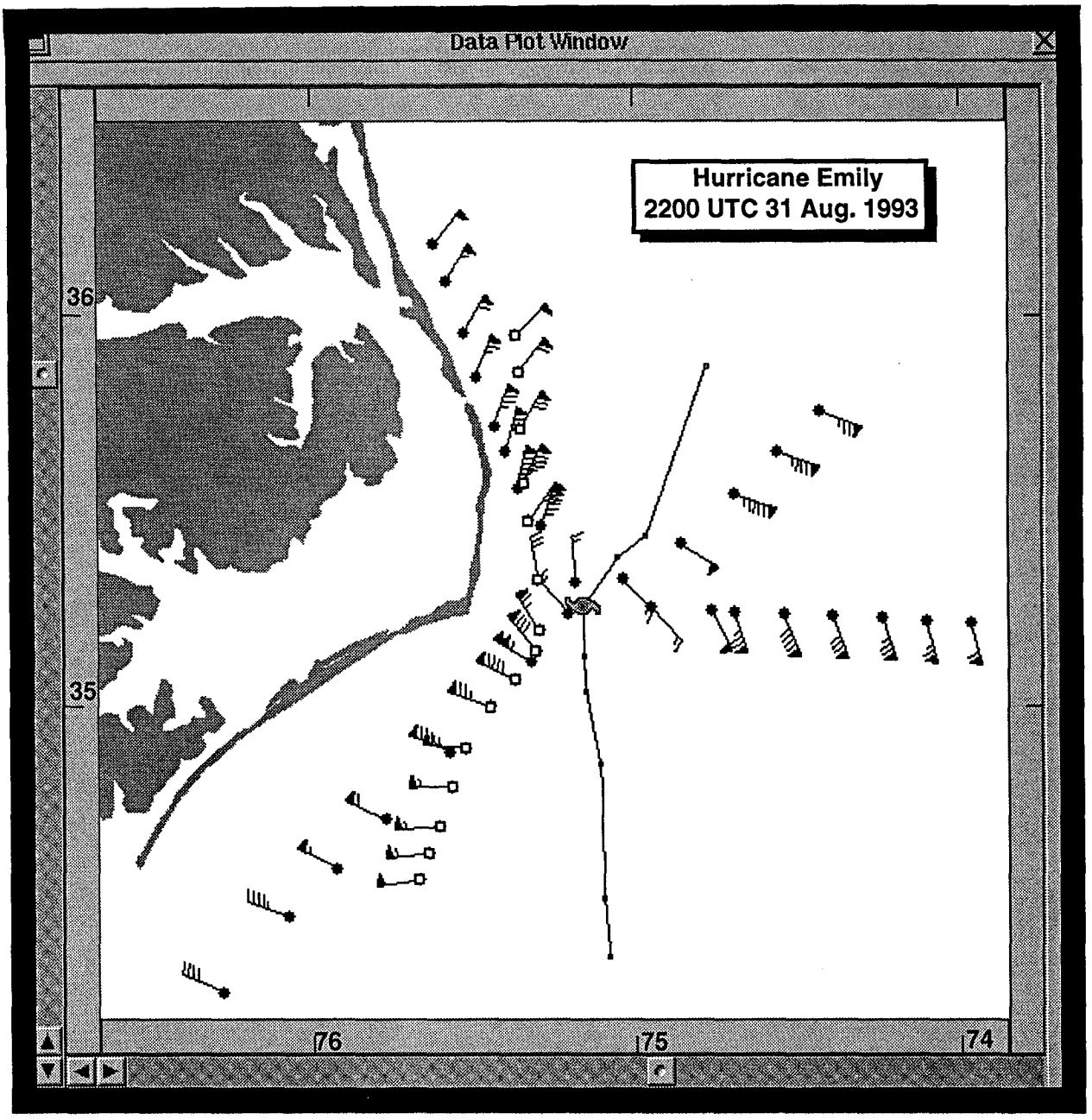

FIG. 5. User interface for the prototype quality control application run on a personal computer at NHC during Hurricane Emily. The window shows surface wind data for Diamond Shoals C-MAN station (open squares) being compared in a storm-relative framework with NOAA research aircraft observations (closed circles) collected in real time and adjusted to the 10-m level. A portion of the storm track is displayed that corresponds to the time interval of the data included in the analysis. The domain is 34.2° to 36.5°N and 73.7° to 76.7°W, and the geography is positioned relative to the storm center for 2200 UTC 31 August 1993. The plotting convention uses a pennant for 25 m s^{-1}, a full barb for 5 m s^{-1}, a half barb for 2.5 m s^{-1}, and an open circle for 1 m s^{-1} wind speeds.

that Emily's strength was maintained as the storm began to recurve to the northeast. The surface wind analyses provide persuasive evidence that a delay in Emily's recurvature of a few hours would have substantially increased the risk to life and property along the outer banks of North Carolina.

d. Synoptic flow experiments

Since 1982, HRD has conducted experiments to determine the wind and thermodynamic fields over oceanic areas within ~1000 km of tropical cyclones in the Atlantic basin. During these synoptic flow experiments, one or two of the NOAA WP-3D research

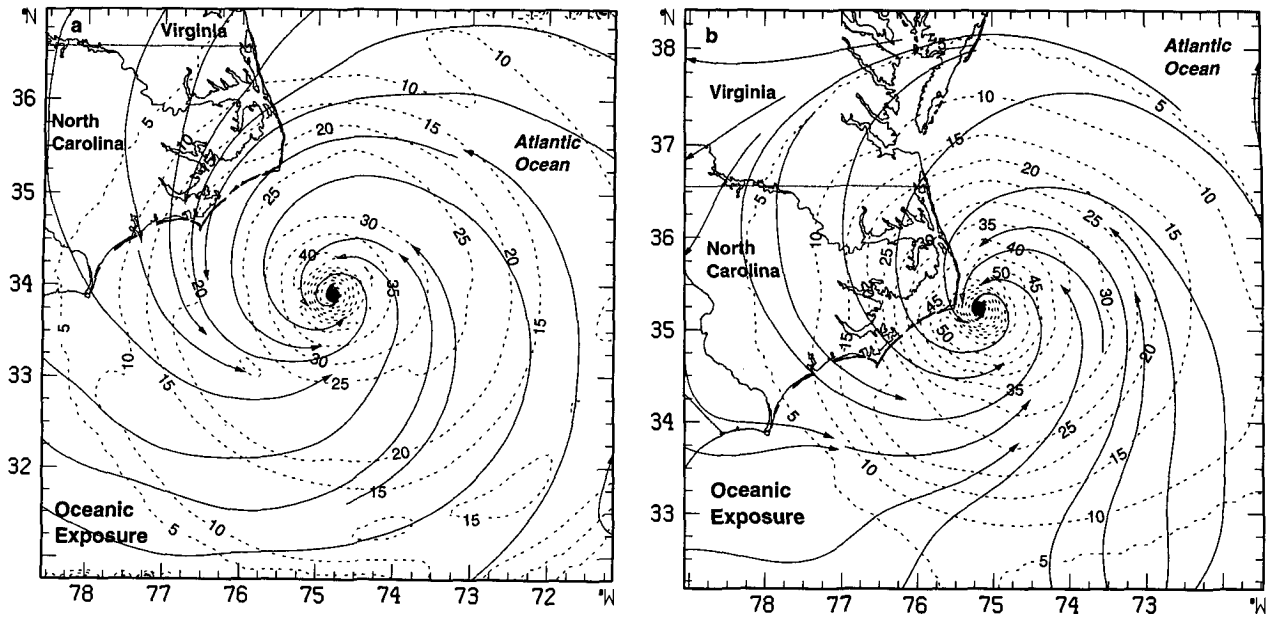

FIG. 6. Real-time streamline and isotach analyses of the V_{ms} field for Hurricane Emily at (a) 1400 and (b) 2200 UTC 31 August 1993. The isotachs (dashed lines) are in meters per second.

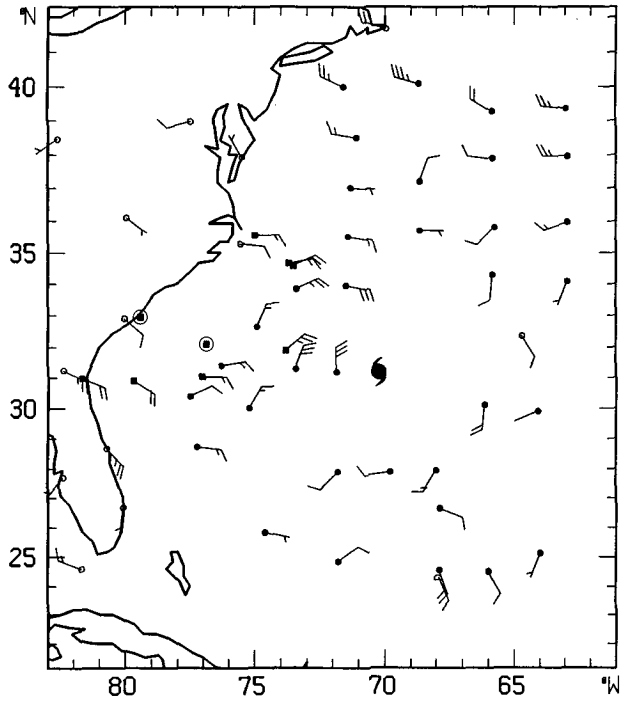

FIG. 7. Midtropospheric operational wind observations in the environment of Hurricane Emily for the 12-h period centered at 0000 UTC 30 August 1993. Observations from 450–600 mb are included in the diagram, although only one observation is shown from each rawinsonde or ODW sounding. Data source is indicated by the plotting symbol as follows: (•) ODWs from the NOAA WP-3D aircraft, (○) rawinsonde, (■) AFRES reconnaissance reports, and (⏢) cloud motion vectors from geosynchronous satellite observations. The wind barb plotting convention is the same as in Fig. 5.

aircraft release Omega dropwindsondes (ODWs) in the hurricane core and environment over a 9–10-h period (Burpee et al. 1984). The ODWs measure pressure, temperature, relative humidity, and wind as they descend from flight level (400–500 mb) to the surface. The ODW data are transmitted in real time to NMC and NHC, where they are incorporated into operational databases. The data are also retained for postflight processing for research purposes.

In a sample of 14 ODW experiments from 1982 to 1989, Franklin and DeMaria (1992) have reported that the ODWs are responsible for statistically significant improvements of 12%–16% in 24–36-h forecasts from VICBAR, a quasi-operational barotropic model discussed in section 3e. Recent work at NMC with the ODW data by one of the coauthors (SJL) has shown a reduction of up to 50% in 12–48-h track forecast errors from NMC's Global Spectral Model for the same sample of cases. ODW-induced improvements in the Global Spectral Model fields consequently produced reduced errors in two other important operational hurricane track forecasting models, the Quasi-Lagrangian Model (QLM; Mathur 1991), and NHC90, a statistical–dynamical model (McAdie 1991). The track forecast improvements due to the ODWs are roughly comparable with the total reduction in normalized NHC official 24-h forecast error occurring over the past 20 years (McAdie and Lawrence 1993).

HRD planned to conduct a synoptic flow experiment about 36–48 h before Emily's landfall or CAL so that the ODWs would be part of the operational data-

base for one of the most critical forecasts. At 1200 UTC 29 August, Hurricane Emily was 900 km from the U.S. coastline. Objective track forecasts from the operational guidance models showed considerable scatter, with some models predicting landfall in North Carolina and others predicting an offshore recurvature. To help forecasters resolve the track uncertainty, HRD conducted a synoptic flow experiment that began at 1800 UTC 29 August. Figure 7 shows the midtropospheric wind observations received operationally at NMC and NHC for the 0000 UTC 30 August analysis cycle, including 35 ODWs obtained by HRD. Without the ODWs, there are only four soundings within 1000 km of the hurricane's center to define Emily's environmental flow.

The ODWs near 36°N, 67°W identify a weakness in the ridge to the north of Emily. The operational VICBAR deep-layer-mean wind analysis for 0000 UTC 30 August, based in part on the ODW data, shows that Emily had passed the longitude of the break in the ridge (Fig. 8). As a result of the change in the direction of the mean flow on the equatorward side of the ridge, Emily turned from a heading toward 330° to one of 285°.

While all of the ODW messages were successfully transmitted to NHC and NMC in real time, software problems at NMC prevented roughly one-third of the ODWs from reaching the objective track forecast models for the 0000 UTC 30 August forecast cycle. Afterward, the software problems were corrected and NMC reran the Global Spectral Model, once using the full ODW dataset and again using none of the ODW data, to assess the ODWs true impact. The forecast tracks from these two runs are shown in Fig. 9. By accurately specifying the strength and structure of the high pressure ridge north of the hurricane, the ODWs improved the forecast with a more accurate initial direction and a recurvature that closely paralleled the actual path of Emily. Forecast errors were reduced by 24%, 64%, and 66% at 24, 48, and 72 h, respectively. These results are similar to the overall impact of the ODWs in the larger sample cited above.

By 1200 UTC 30 August, NHC had issued a hurricane watch from South Carolina to Delaware, but recurvature before landfall was still possible. The future track depended on the midtropospheric anticyclone to Emily's northwest, which was forecast to move eastward and weaken. Faced with this situation, the director of NHC requested that HRD conduct a second ODW mission. The flight successfully acquired ODW data north of the hurricane (Fig. 10). The ODW observations confirmed that the anticyclone had moved just offshore, and that Emily was about to pass the longitude of the high center. With this information, forecasters were able to predict confidently that Emily would recurve after bringing hurricane force winds to the outer banks but would not affect the highly populated northeastern U.S. coastline. The dropwindsondes helped NHC to pinpoint Emily's position relative to the upper-level ridge and thereby issue accurate warnings for residents and vacationers along the eastern seaboard. The ODW data on this flight were acquired for less than $50,000 and may have saved several million dollars in preparedness costs for coastal communities not included in the warning area.

e. Track model

A barotropic hurricane track forecast package known as VICBAR has been run operationally at HRD since 1989 (DeMaria et al. 1992). VICBAR consists of an objective analysis scheme and a prediction model, both based upon the SAFER technique on nested domains, and is competitive with the other operational hurricane track forecast models (Aberson and DeMaria 1994). It produced track forecasts at 6-h intervals from the time that NHC classified Emily as a depression until the storm became extratropical.

Model track forecasts are verified by comparison with the NHC best track. The absolute error is the great-circle distance between a forecast and its best-

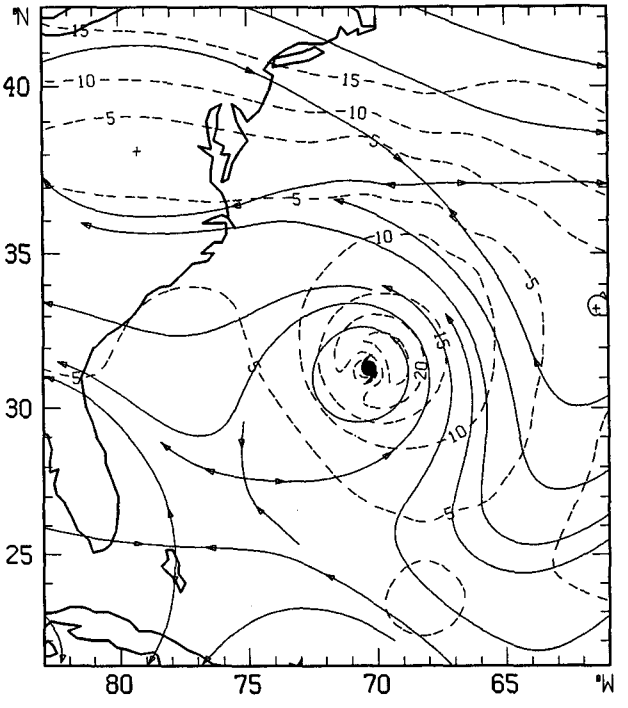

FIG. 8. Operational VICBAR analysis of the 200–850-mb deep-layer-mean wind flow for 0000 UTC 30 August 1993. Isotachs (dashed lines) are given every 5 m s^{-1}. Anticyclonic circulation centers are indicated by the "+" symbols near 38°N, 79°W and 33°N, 61°W.

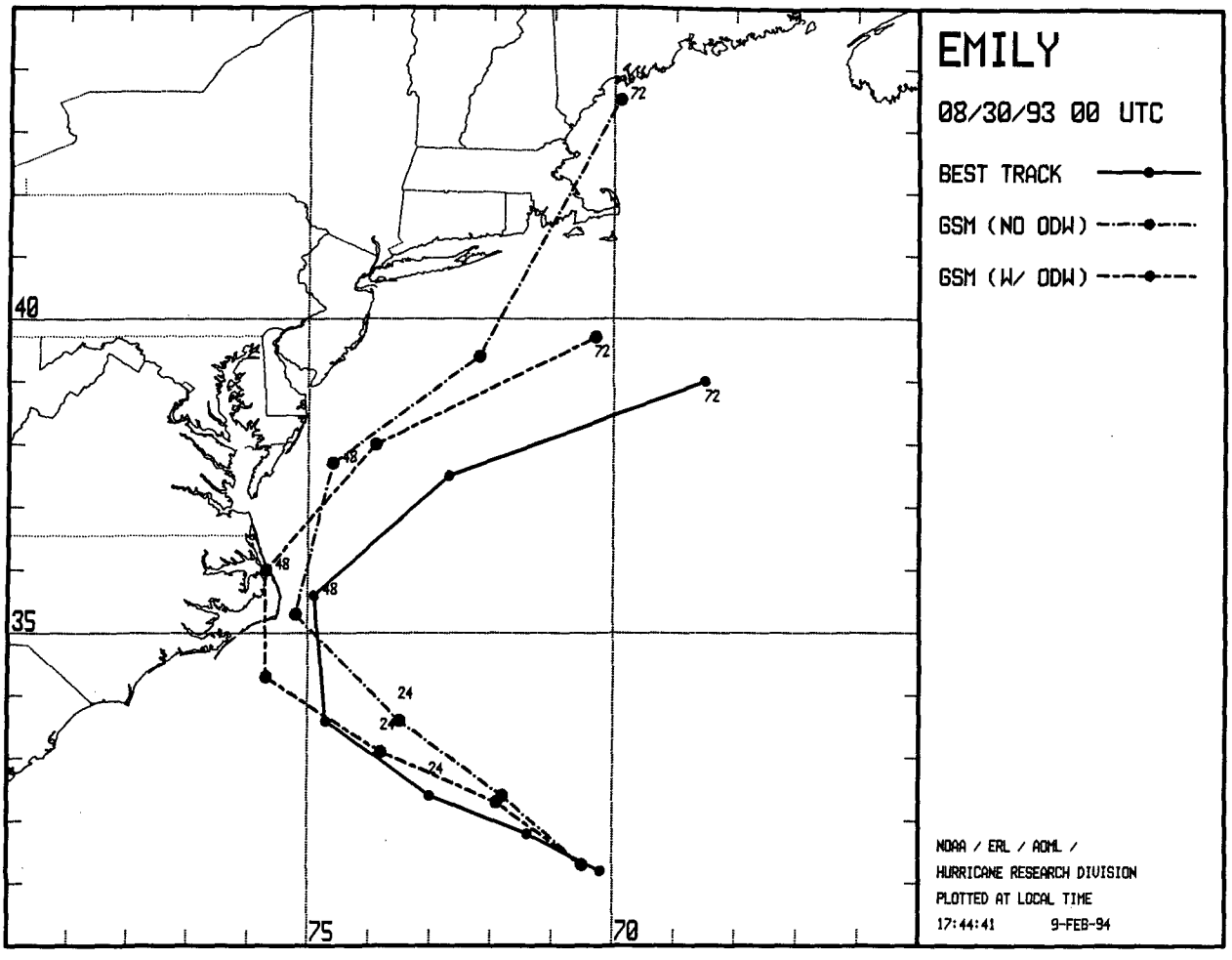

FIG. 9. Verifying best-track (solid) and Global Spectral Model forecast tracks run with the ODWs (dashed) and without the ODWs (dotted–dashed) for Emily at 0000 UTC 30 August 1993. Actual and forecast positions are given at 12-h intervals.

track position. The relative error is the difference between the absolute errors of a forecast and the corresponding CLIPER forecast, a simple statistical model with climatological and persistence predictors (Neumann 1972), divided by the CLIPER error. Forecasts with negative relative error are defined as skillful.

Figure 11 compares the relative errors of VICBAR for Emily with the other operational hurricane track forecast models. To reduce potential biases, the figures include only "fair" comparisons of forecasts based upon the same global analysis and model run cycle. The 0000 and 1200 UTC sample has fewer cases than the 0600 and 1800 UTC sample because several models (Aviation,[1] QLM, and NHC90-LATE) were not always available at that time. The VICBAR forecasts have considerable skill (over 30% except at 12 h) and were competitive with the other operational hurricane track models during Emily, especially for shorter-range forecasts. This skill was only 5% higher during Emily than for all other storms during the 1993 hurricane season.

Figure 12 shows the accuracy of the predictions of the distance to the CAL of each operational track forecast model. The initial and forecast positions of each model are fitted with cubic splines, and the distance to the CAL is found. VICBAR errors in the prediction of the distance to the CAL were almost always smaller and more consistent than those of the other operational models. This result confirms that VICBAR was one of the best operational models during preparation of the important forecasts before Hurricane Emily affected the North Carolina coastline.

f. Intensity change model

Forecasters at NHC rely on tropical cyclone track guidance that ranges from the relatively simple CLIPER model, to complex two- and three-dimensional re-

[1] A version of the NMC Global Spectral Model that completes its 72-h forecast about 6 h after the synoptic time.

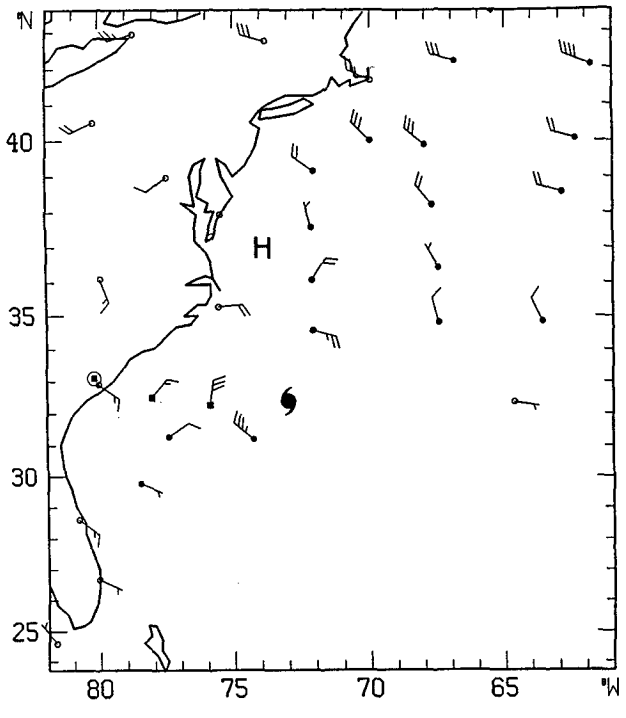

FIG. 10. Midtropospheric operational wind observations as in Fig. 7 but for the 12-h period centered at 0000 UTC 31 August 1993.

gional dynamical models like VICBAR and the QLM, and finally to multilevel global models from national centers. In contrast, the only operational guidance for tropical cyclone intensity prediction is SHIFOR, a model based upon climatology and persistence information (Jarvinen and Neumann 1979).

Recently, DeMaria and Kaplan (1994) developed a statistical hurricane intensity prediction scheme (SHIPS) that forecasts the maximum sustained surface wind speed at 12-h intervals out to 72 h. SHIPS includes synoptic as well as climatological and persistence predictors. The synoptic predictors were derived from 0000 and 1200 UTC analyses produced by the VICBAR analysis and prediction model discussed in section 3e. The developmental database for SHIPS consisted of all named Atlantic storms from 1989 to 1992 and a few storms from 1982 to 1988 for forecast periods when a storm remained over water. Standard multiple regression techniques selected predictors whose correlation with future intensity changes was statistically significant at the 95% level for at least one forecast time. Table 3 lists the ten predictors that satisfied this criterion and the predominant sign of the correlation of each predictor with intensity change. Seven of the predictors, including four of the first five selected, are synoptic; three represent climatology or persistence. DeMaria and Kaplan (1994) provide detailed information on the SHIPS predictors.

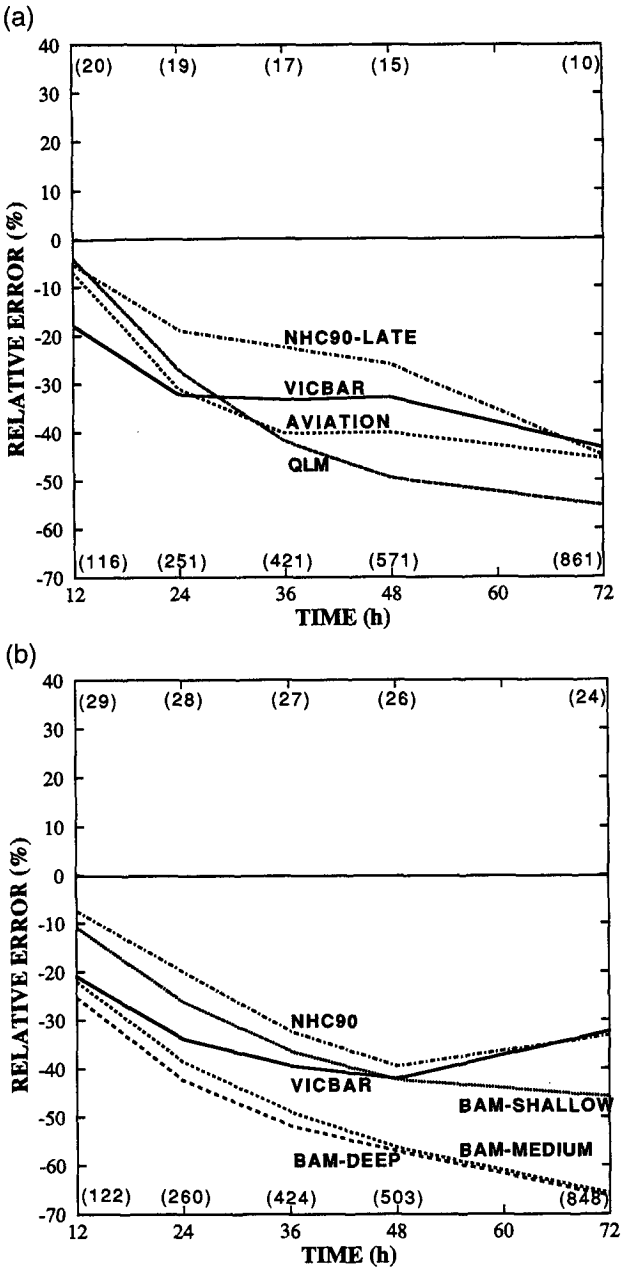

FIG. 11. "Fair" comparisons between VICBAR and (a) Aviation, QLM, and NHC90-LATE at 0000 and 1200 UTC, and (b) the three BAM models (Marks 1992) and NHC90 at 0600 and 1800 UTC, for Hurricane Emily. Errors are percentages relative to CLIPER forecast errors. The numbers in parentheses at the top are the number of cases in each homogeneous sample; the numbers in parentheses at the bottom are the absolute errors of CLIPER (km).

SHIPS was run operationally at 6-h intervals during the 1993 Atlantic hurricane season. Figure 13 shows the 1200 UTC SHIFOR and SHIPS intensity forecasts for Emily; similar results were obtained for the other forecast times (not shown). Both SHIPS and SHIFOR forecast Emily's first intensification from 25 to 26

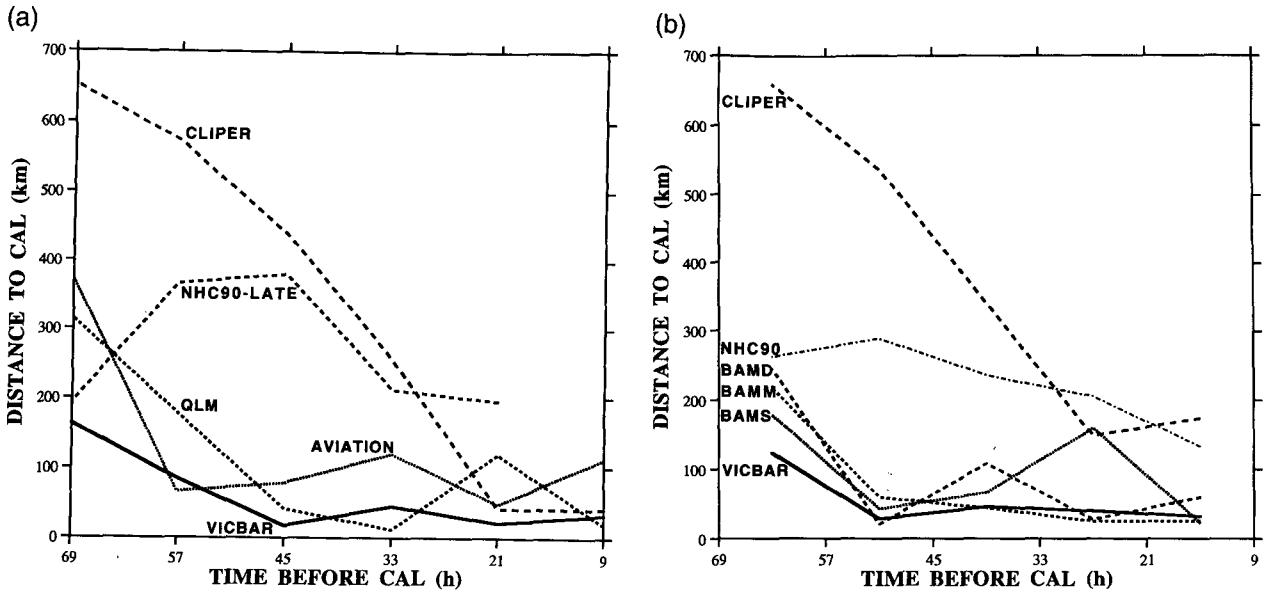

FIG. 12. "Fair" comparison of the smallest distance between each forecast track and the closest point to landfall for (a) Aviation, QLM, and NHC90-LATE at 0000 and 1200 UTC, and (b) the three BAM models and NHC90 at 0600 and 1800 UTC, for Hurricane Emily. Missing forecasts are not shown.

August. Although SHIPS was premature in forecasting the intensification, it was more accurate than SHIFOR in predicting the magnitude of the increase. The ability of SHIPS to account for the lower than average vertical shear in Emily's near environment was likely responsible for this improvement.

From 26 to 30 August, SHIPS forecasts wind speed increases of up to 20 m s^{-1}, while SHIFOR more accurately forecasts only slight strengthening. Two factors likely contributed to SHIPS overpredicting the rate of intensification. First, a gap in aircraft reconnaissance (M. Lawrence 1993, personal communication) resulted in erroneous operational intensity estimates on 26 and 27 August. These erroneous intensity estimates led to anomalously large values of the persistence term (DVMX) that accounted for several forecasts of excessive intensification on these dates. Second, SHIPS presently does not account for evolution of the synoptic environment during the forecast period, and it was therefore unable to predict the increased vertical shear (SHR) caused by the interaction of Emily with an upper-level trough to the northwest of the storm. These artificially low values of vertical shear caused SHIPS to overpredict the intensification.

Emily began to intensify more rapidly at midday on 30 August. The onset of this period of intensification was likely delayed due to Emily's interaction with the upper-level trough. Although this interaction produced positive 200-mb planetary and relative eddy fluxes (PEFC and REFC) normally favorable for intensification, it also increased the vertical shear, which may have precluded any substantial strengthening. After reaching its peak intensity, Emily weakened rapidly as it moved north and then

TABLE 3. Synoptic (S) and climatological and persistence (CP) predictors used in SHIPS along with their corresponding acronyms. Predictors are listed in descending order of importance. The predominant sign of the correlation of each predictor with intensity change is also indicated. Julian day 253 is 10 September in nonleap years.

Maximum possible intensity—initial intensity	POT	S	+
Magnitude of 850–200-mb vertical shear	SHR	S	−
Intensity change during previous 12 h	DVMX	CP	+
200-mb relative eddy angular momentum flux convergence	REFC	S	+
200-mb planetary eddy angular momentum flux convergence	PEFC	S	+
Absolute value of (Julian day − 253)	JDATE	CP	−
Initial storm longitude (°W)	LONG	CP	+
Distance to nearest major landmass	DTL	S	+
850-mb relative angular momentum	SIZE	S	+
Time tendency of vertical shear magnitude	DSHR	S	−

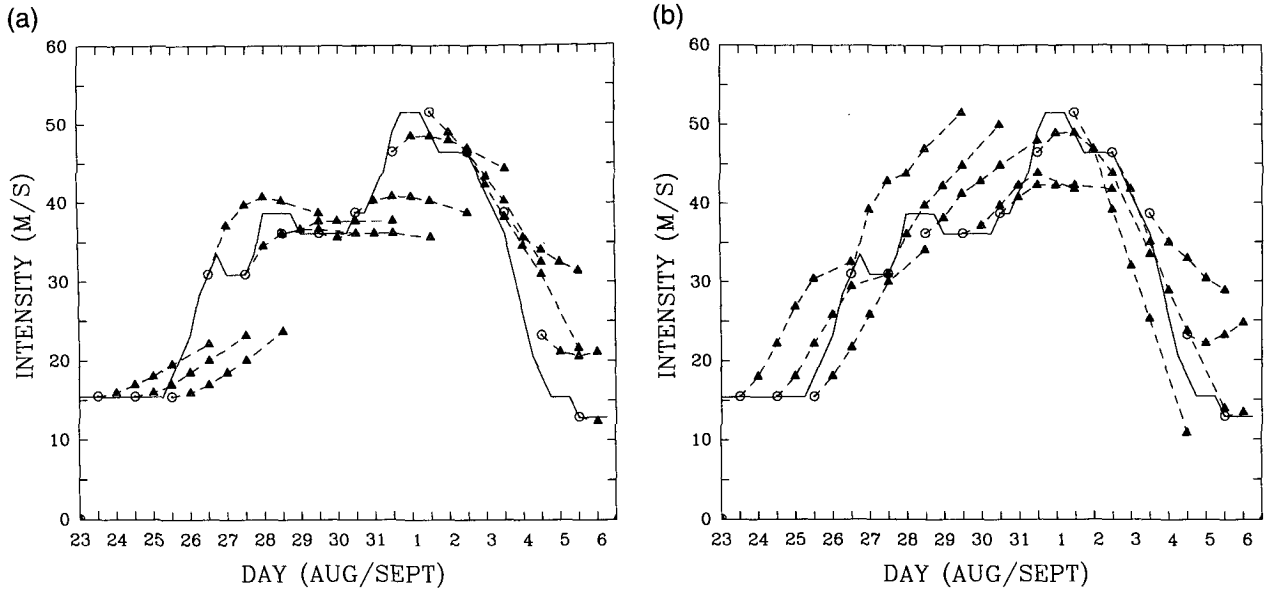

FIG. 13. The poststorm intensity estimates (solid line) for 0000 and 1200 UTC and the operational forecasts at 1200 UTC for (a) SHIFOR and (b) SHIPS. The operational intensities at each initial time are indicated by open circles, and the model forecast intensities at 12, 24, 36, 48, and 72 h are denoted by triangles. The dashed lines connect the forecasts for a given initial time.

northeastward over cooler water into an area with increasing vertical shear. This period of weakening was reasonably well forecast by both SHIPS and SHIFOR, although SHIPS was somewhat better in forecasting the magnitude of the decrease.

Table 4 contains a homogeneous comparison of the operational SHIPS and SHIFOR intensity forecast errors for Emily and the error statistics for the no change (NCHG) model that assumes a storm's intensity will remain constant during the forecast period. The average SHIPS errors were smaller than those of the NCHG model at all forecast times except 12 h. In addition, the SHIPS errors were smaller than the SHIFOR errors at 48 and 72 h, but were slightly larger at 12–36 h. Statistical significance tests were performed to determine whether the SHIPS errors were significantly different from those of the NCHG and SHIFOR models when the sample sizes were corrected to account for serial correlation between forecasts. The results show that the differences between the SHIPS errors and those of the NCHG and SHIFOR models are not statistically significant from 12–48 h. The SHIPS errors, however, are significantly different than those of the SHIFOR (NCHG) model at the 95% (99%) level at 72 h.

The error statistics for Emily differ from the larger data sample of DeMaria and Kaplan (1994), which indicated that SHIPS errors were smaller than SHIFOR errors at all forecast times, with the largest improvement at 48 h. These improvements were shown to be statistically significant at the 95% level at 12 and 72 h and the 99% at 24–48 h. Evaluation of real-time intensity forecasts from the 1993 season shows that SHIPS had 10%–15% skill relative to SHIFOR. SHIPS is the first intensity forecast model in the Atlantic basin to have demonstrated skill in an operational setting. In the absence of adequate guidance models, NHC's official intensity forecasts have had little skill out to 72 h, the longest forecasts issued to the public.

4. Concluding discussion

HRD achieved three important accomplishments for the first time during Hurricane Emily. It successfully transmitted a series of radar composites from the research aircraft to NHC while the storm was beyond the range of land-based radars. The radar composites allowed forecasters to see the horizontal patterns of precipitation and interpret flight-level thermodynamic

TABLE 4. Average absolute errors ($m\ s^{-1}$) and number of forecasts (N) during Emily at each forecast interval for the SHIFOR, SHIPS, and NCHG models.

	Forecast interval (h)				
Model	**12**	**24**	**36**	**48**	**72**
SHIFOR	3.2	4.9	6.0	7.5	9.3
SHIPS	3.4	5.6	6.8	7.4	6.0
NCHG	2.9	5.7	8.3	10.9	14.9
N	57	55	53	51	46

and kinematic observations relative to the eyewall and rainbands. In addition, researchers completed five streamline and isotach analyses of the surface wind field in real time as Emily's eye approached and passed just offshore from the eastern barrier islands of North Carolina. The data processing package assimilated the wind observations from a variety of platforms at different heights and with nonuniform averaging times. The processing algorithms standardized the data to 10 m and estimated the maximum sustained 1-min average wind speed and direction. The third accomplishment was the transition of the ODW synoptic flow experiment to a program capable of supporting operational hurricane requirements. NHC made its first request for an ODW flight as Emily neared North Carolina. The dropwindsonde data from this flight helped forecasters correctly predict that Emily's eye would remain offshore and recurve without striking land.

HRD has recorded digital reflectivity data from coastal WSR-57 radars during the landfall of hurricanes since the middle 1970s. Radar specialists have transported portable recorders from Miami to the NWS coastal radars on either side of a projected landfall, helped the local electronics technicians connect the recorders to the radar, and recorded the reflectivity data on magnetic tapes. Parrish et al. (1982) and Burpee and Black (1989) used these data to describe mesoscale and convective-scale features in the eyewall and inner rainbands of three hurricanes. Dodge et al. (1987, 1993) animated and narrated color time-lapse videos of the reflectivity and distributed them to NWS offices. The videos illustrate characteristic hurricane reflectivity patterns during landfall and help educate forecasters at coastal stations rarely affected by hurricanes. The radar data have also provided ground truth for algorithms that estimate tropical cyclone rainfall from satellite information. Unfortunately, the recorder taken to Cape Hatteras failed to operate as the center of Emily passed offshore. Researchers are, nevertheless, continuing to describe hurricane precipitation patterns based upon WSR-57 reflectivity analyses and are changing analysis procedures to include the new WSR-88D (Weather Surveillance Radar–1988 Doppler) data. Joint land-based and airborne Doppler radar experiments are being planned.

The real-time hurricane data analyses and forecast models described here for Emily are representative of HRD's ongoing support for NHC that began after the collocation of the two groups in 1959. Even though programmatic cutbacks forced HRD to move to a building 15 km from NHC in 1983, researchers and forecasters have continued to work together to improve warnings and predictions. High-speed transfers of digital information now provide HRD with real-time access to operational datasets that were unavailable outside of NWS forecast centers a few years ago. Meetings involving both organizations have been easily arranged because NHC is on the commuting route of nearly all HRD researchers. In 1995, however, NHC plans to move to a location about 35 km from HRD that is not near any of the commuting routes of the researchers. This move will present new obstacles to technology transfer that HRD and NMC will minimize by implementing state-of-the-art data transfers and conferencing capabilities to help diminish the effect of the separation distance.

Future observational and analysis research will develop more algorithms for the analysis of airborne and land-based radar reflectivity and Doppler velocities, implement algorithms to estimate surface winds from airborne remote sensing instrumentation, increase the availability of surface wind analyses, improve the quality and quantity of aircraft data in the hurricane core and periphery, and evaluate NMC analyses and forecasts in the Tropics. Modeling efforts will include the development of a three-dimensional hurricane track model that uses the SAFER numerical methods, research on the prediction of the accuracy of track forecasts, and the addition of NMC forecast model predictors that incorporate synoptic-scale and postlandfall changes in the SHIPS regression model.

Acknowledgments. The authors thank Stan Goldenberg and Chris Samsury of HRD, Lixion Avila of NHC, and Ron Lavoie of NWS's Office of Meteorology, who reviewed an earlier version of the manuscript. The flight crews of the NOAA WP-3D research planes and the AFRES reconnaissance aircraft obtained most of the data used in sections 3a–d. Cary Bakker, Bill Barry, Joyce Berkeley, Kevin Day, Neal Dorst, Nancy Griffin, Bob Kohler, Paul Leighton, and Ed Rahn of HRD provided plotting and software support for the surface and ODW wind analyses and the display of the radar reflectivity composites. Special thanks to Eric Meindl of NDBC for his efforts in adding the continuous wind measurements to the real-time data records for moored buoys and C-MAN platforms. Peter Dodge of HRD described his experiences with the WSR-57 radar recorder at Cape Hatteras, Mike Black provided some of the software for the statistical significance tests, and Gail Derr processed the manuscript.

References

Aberson, S. D., and M. DeMaria, 1994: Verification of a nested barotropic hurricane track forecast model (VICBAR). *Mon. Wea. Rev.*, in press.

Burpee, R. W., and M. L. Black, 1989: Temporal and spatial variations of rainfall near the centers of two tropical cyclones. *Mon. Wea. Rev.*, **117**, 2204–2218.

——, D. G. Marks, and R. T. Merrill, 1984: An assessment of omega dropwindsonde data in track forecasts of Hurricane Debby (1982). *Bull. Amer. Meteor. Soc.*, **65**, 1050–1058.

DeMaria, M., and J. Kaplan, 1994: A statistical hurricane intensity

prediction scheme for the Atlantic basin. *Wea. Forecasting,* **9,** 209–220.

——, S. D. Aberson, K. V. Ooyama, and S. J. Lord, 1992: A nested spectral model for hurricane track forecasting. *Mon. Wea. Rev.,* **120,** 1628–1643.

Dodge, P., M. Black, B. Burpee, and F. Marks, 1987: Time-lapse radar imagery from landfalling hurricanes. Preprints, *17th Conf. on Hurricanes and Tropical Meteorology,* Miami, FL, Amer. Meteor. Soc., 166–169.

——, ——, P. Leighton, B. Christoe, F. Marks Jr., and R. Burpee, 1993: Time-lapse radar images of Hurricane Andrew's landfalls. Preprints, *20th Conf. on Hurricanes and Tropical Meteorology.* San Antonio, TX, Amer. Meteor. Soc., 163–166.

Dunn, G. E., R. C. Gentry, and B. M. Lewis, 1968: An eight-year experiment in improving forecasts of hurricane motion. *Mon. Wea. Rev.,* **96,** 708–713.

Franklin, J. L., and M. DeMaria, 1992: The impact of Omega dropwindsonde observations on barotropic hurricane track forecasts. *Mon. Wea. Rev.,* **120,** 381–391.

Gentry, R. C., 1980: History of hurricane research in the United States with special emphasis on the National Hurricane Research Laboratory and associated groups. Selected papers, *13th Tech. Conf. on Hurricanes and Tropical Meteorology,* Miami, FL, Amer. Meteor. Soc., 6–16.

Griffin, J. S., R. W. Burpee, F. D. Marks Jr., and J. L. Franklin, 1992: Real-time airborne analysis of aircraft data supporting operational hurricane forecasting. *Wea. Forecasting,* **7,** 480–490.

Jarvinen, B. R., and C. J. Neumann, 1979: Statistical forecasts of tropical cyclone intensity. NOAA Tech. Memo. NWS NHC-10, 22 pp. [Available from NHC, 1320 S. Dixie Highway, Coral Gables, FL 33146–2976.]

Kurihara, Y., M. A. Bender, R. E. Tuleya, and R. J. Ross, 1993: Hurricane forecasting with the GFDL automated prediction system. Preprints, *20th Conf. on Hurricanes and Tropical Meteorology,* San Antonio, TX, Amer. Meteor. Soc., 323–326.

Liu, W. T., K. B. Katsaros, and J. A. Businger, 1979: Bulk parameterizations of air–sea exchanges of heat and water vapor including the molecular constraints at the interface. *J. Atmos. Sci.,* **36,** 1722–1735.

Lord, S. J., 1991: A bogusing system for vortex circulation in the National Meteorological Center global forecast model. Preprints, *19th Conf. on Hurricanes and Tropical Meteorology,* Miami, FL, Amer. Meteor. Soc., 328–330.

Marks, D. G., 1992: The beta and advection model for hurricane track forecasting. NOAA Tech. Memo. NWS NMC 70, 89 pp. [Available from NMC/NOAA, World Weather Building, Washington, DC 20233.]

Marks, F. D., Jr., 1985: Evolution of the structure of precipitation in Hurricane Allen (1980). *Mon. Wea. Rev.,* **113,** 909–930.

Mathur, M. B., 1991: The National Meteorological Center's quasi-Lagrangian model for hurricane prediction. *Mon. Wea. Rev.,* **119,** 1419–1447.

McAdie, C. J., 1991: A comparison of tropical cyclone track forecasts produced by NHC90 and an alternate version (NHC90A) during the 1990 hurricane season. *Proc. 19th Conf. on Hurricanes and Tropical Meteorology,* Miami, FL, Amer. Meteor. Soc., 290–294.

——, and M. B. Lawrence, 1993: Long-term trends in National Hurricane Center track forecast errors in the Atlantic basin. Preprints, *20th Conf. on Hurricanes and Tropical Meteorology,* San Antonio, TX, Amer. Meteor. Soc., 281–284.

Miller, B. I., E. C. Hill, and P. P. Chase, 1968: Revised technique for forecasting hurricane motion by statistical methods. *Mon. Wea. Rev.,* **96,** 540–548.

Neumann, C. J., 1972: An alternate to the HURRAN tropical cyclone forecast system. NOAA Tech. Memo. NWS SR-62, 22 pp. [Available from NHC, 1320 S. Dixie Highway, Coral Gables, FL 33146–2976.]

——, 1981: Trends in forecasting of Atlantic tropical cyclones. *Bull. Amer. Meteor. Soc.,* **62,** 1473–1485.

Ooyama, K. V., 1987: Scale controlled objective analysis. *Mon. Wea. Rev.,* **115,** 2479–2506.

Parrish, J. R., R. W. Burpee, F. D. Marks Jr., and R. Grebe, 1982: Rainfall patterns observed by digitized radar during the landfall of Hurricane Frederic (1979). *Mon. Wea. Rev.,* **110,** 1933–1944.

Pifer, B., M. Zimmer, J. DuGranrut, and J. McFadden, 1978: Aircraft satellite data link. *Bull. Amer. Meteor. Soc.,* **59,** 288–290.

Powell, M. D., 1980: Evaluations of diagnostic marine boundary layer models applied to hurricanes. *Mon. Wea. Rev.,* **108,** 757–766.

——, P. P. Dodge, and M. L. Black, 1991: The landfall of Hurricane Hugo in the Carolinas: Surface wind distribution. *Wea. Forecasting,* **6,** 379–399.

Samsury, C. E., and E. N. Rappaport, 1991: Predicting Atlantic hurricane intensity from research and reconnaissance aircraft data. Preprints, *19th Conf. on Hurricanes and Tropical Meteorology,* Miami, FL, Amer. Meteor. Soc., 516–520.

Sanders, F., and R. W. Burpee, 1968: Experiments in barotropic hurricane track forecasting. *J. Appl. Meteor.,* **7,** 313–323.

Shapiro, L. J., and H. E. Willoughby, 1982: The response of balanced hurricanes to local sources of heat and momentum. *J. Atmos. Sci.,* **39,** 378–394.

Simpson, R. H., 1980: Implementation phase of the National Hurricane Research Project. Selected papers, *13th Tech. Conf. on Hurricanes and Tropical Meteorology,* Miami, FL, Amer. Meteor. Soc., 1–5.

——, and H. Riehl, 1981: *The Hurricane and Its Impact.* Louisiana State University Press, 398 pp.

Willoughby, H. E., 1990: Temporal changes in the primary circulation in tropical cyclones. *J. Atmos. Sci.,* **47,** 242–264.

——, and W. P. Barry, 1987: Real-time data acquisition and analysis in Hurricane Charley of 1986. *Extended Abstracts, 17th Conf. on Hurricanes and Tropical Meteorology,* Miami, FL, Amer. Meteor. Soc., 341–342.

——, J. A. Clos, and M. G. Shoreibah, 1982: Concentric eye walls, secondary wind maxima, and the evolution of the hurricane vortex. *J. Atmos. Sci.,* **39,** 395–411.

——, F. D. Marks Jr., and R. J. Feinberg, 1984: Stationary and moving convective bands in hurricanes. *J. Atmos. Sci.,* **41,** 3189–3211.

——, W. P. Barry, and M. E. Rahn, 1989: Real-time monitoring of Hurricane Gilbert. Preprints, *18th Conf. on Hurricanes and Tropical Meteorology,* San Diego, CA, Amer. Meteor. Soc., 220–221.